ACS APPLIED MATERIALS & INTERFACES

Research Article

www.acsami.org

Rational Surface Engineering of Anatase Titania Core–Shell Nanowire Arrays: Full-Solution Processed Synthesis and Remarkable Photovoltaic Performance

Wu-Qiang Wu, Hao-Lin Feng, Hua-Shang Rao, Dai-Bin Kuang,* and Cheng-Yong Su

MOE Key Laboratory of Bioinorganic and Synthetic Chemistry, KLGHEI of Environment and Energy Chemistry, Lehn Institute of Functional Materials, State Key Laboratory of Optoelectronic Materials and Technologies, School of Chemistry and Chemical Engineering, Sun Yat-sen University, Guangzhou 510275, P. R. China

Supporting Information

ABSTRACT: The high-performance of a well-aligned 1D nanostructured electrode relies largely on a smart and rational modification with other active nanomaterials. Herein, we present a facile solution-based route to fabricate a well-aligned metal oxide-based core–shell hybrid arrays on TCO substrate. Demonstrated samples included nanowire@nanoparticle (TNW@NP) or nanowire@nanosheet (TNW@NS) with a unique porous core/shell nanowire arrays architecture in the absence or presence of DETA during the solvothermal treatment process. The "alcoholysis" and "ripening" growth mechanism is proposed to explain the formation of honeycomb-like nanosheets shell on nanowires core. Based on careful control of experimental condition, a novel double layered TiO_2 photoanode (DL-TNW@NS-YSHTSs) consisting of 16 μm thick TNW@NS under layer and 6 μm thick yolk–shell hierarchical TiO_2 microspheres (YSHTSs) top layer can be obtained, exhibiting an impressive PCE over 10% at 100 mW cm^{-2}, which can be attributed to the well-organized photoanode composed of hierarchical core–shell arrays architecture and yolk–shell hollow spheres architecture with synergistic effects of high dye loading and superior light scattering for prominent light harvesting efficiency.

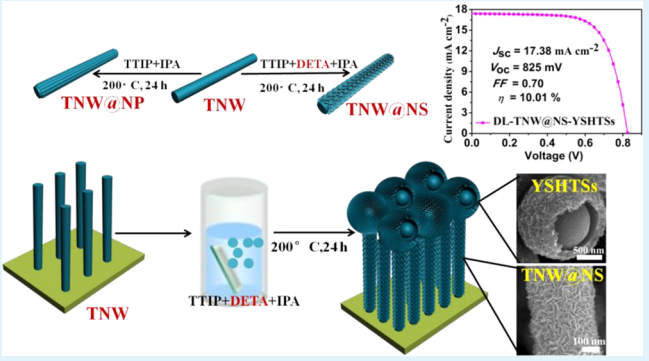

KEYWORDS: *solar cells, nanowires, nanosheets, core–shell, electron transport*

INTRODUCTION

Hierarchical assembly of hybrid nanostructures has gained tremendous scientific and technological interests due to their high versatility and applicability as essential components in Li-ion batteries, solar cells, gas sensors, water splitting, pollutants degradation and field emission, etc.[1−5] In recent years, considerable effort has been concentrated on integrating the metal oxide materials, for instance, TiO_2, ZnO, SnO_2, Nb_2O_5, Zn_2SnO_4, etc., into core–shell hybrid architectures with homogeneous or heterogeneous composite-like nanostructure according to the "band-structure matching" strategy, which would exhibit fascinating synergistic and complementary properties (enhanced electrical, optical, electrochemical performance) or multifunctionalities with respect to the single component counterparts.[6−11] Complex hybrid structures, for example, ZnO-TiO_2,[12] SnO_2–TiO_2,[13,14] Zn_2SnO_4–ZnO,[15] and SnO_2–ZnO[16] have been reported. Among various types of semiconductor materials, TiO_2, plays a crucial role, and is widely recognized as the most promising and versatile candidate for the fabrication of TiO_2-based hybrid photoanodes when applied in dye-sensitized solar cells (DSSCs), especially because of its appropriate electronic band structure and remarkable chemical stability.[17−19]

More recently, DSSCs employing the one-dimensional (1D) nanostructures such as nanowires (NWs), nanotubes (NTs), nanorods (NRs), and nanofibers (NFs) emerged as a promising alternative to prototype nanoparticles (NPs) based devices, as they offer a direct pathway for photogenerated electrons to transport along the long axis of 1D nanostructures, thereby efficiently boosting charge transport and markedly improving the charge collection efficiency.[20−27] However, the device performance of DSSC exploiting the 1D nanostructured photoanode still lagged behind the standard mesoporous nanocrystalline photoanode mainly due to severe limitations of insufficient surface area which led to limited dye adsorption capacity and thus translated to lower generated photocurrents.[28] A common strategy for improving the dye loading capability is to coat 1D nanostructures with a large number of small-sized nanoparticles, which would enhance the power

Received: July 31, 2014
Accepted: October 14, 2014
Published: October 14, 2014

conversion efficiency of DSSCs.[29,30] However, more often than not, such route would largely sacrifice the electron lifetime of DSSCs, which is ascribed from a large charge recombination loss within disordered network of outside nanoparticles where the electron trapping and scattering occur frequently at numerous grain boundaries and thus made it difficult to collect electrons from nanoparticles. Another approach for enhancing the efficiency of 1D nanostructure-based DSSCs is to decorate 1D nanostructures with dendritic NRs branches[31−35] or 2D lamellar nanosheets (NSs).[14,36] In this case, the NRs or lamellar NSs branches could not only enhance the specific surface area but also improve the light scattering, while simultaneously maintain the fast electron transfer characteristics. In particular, owing to the high surface area and excellent electrical conductivity of 2D NS structures, thin NSs-based hybrid photoanodes were preferred. So far, few successful examples have been reported for the fabrication of well-aligned core−shell hybrid nanoarrays with homostructures (all TiO_2 components) with precise structural control and tunable functions through a simple and cost-effective method, let alone its application in solar energy conversion.

Herein, for the first time, we report a facile, simple but powerful two-step full solution-processed strategy to fabricate well-aligned anatase TiO_2 NW-NS core−shell hybrid nanoarrays (referred to here as TNW@NS) directly on transparent conducting glass. These NW-NS core−shell nanoarrays structures were crafted by subjecting oriented TNW arrays backbone to the solvothermal reaction in the mixed solution containing titanium isopropoxide (TTIP), isopropanol (IPA), and diethylenetramine (DETA). While in the absence of DETA, nanoparticles modified core−shell nanoarrays were obtained (referred to here as TNW@NP). As a proof-of-concept application, these core−shell hybrid nanoarrays were used as the photoanodes of DSSCs for solar energy conversion. DSSCs using TNW@NS photoanodes exhibited a markedly enhanced power conversion efficiency (PCE) of 8.67% (i.e., a 70% increase in PCE as compared to the devices prepared by using pure TNW with PCE of 5.09%), which due primarily to the synergistic effect of high dye loading, superior light scattering, and moderate electron transport of such core−shell TNW@NS photoelectrodes. Interestingly, by changing the TNW/FTO film from facing-down side to facing-up side, an unique double layered photoanode consisting of 16 μm TNW@NS under layer and 6 μm thick yolk−shell hierarchical TiO_2 spheres (YSHTSs) top layer was obtained and DSSC based on it yielded an impressive PCE over 10%. To the best of our knowledge, no reports have been published on such simple and easy-to-operate route to synthesize honeycomb-like NSs encircled TNW core−shell nanoarrays while simultaneously enabling the deposition of YSHTSs scattering units onto the top, leading to the construction of such efficient double layered photoanode.

EXPERIMENTAL SECTION

Fabrication of 1D TNW Arrays via the Hydrothermal Process. First, TiO_2 blocking layer[37] (100 nm in thickness) was spin-coated on the FTO glass substrate (2.5 cm × 3 cm), which had been cleaned with acetone, ethanol, water, respectively. On top of the blocking layer coated FTO, well-aligned TNW arrays were hydrothermally grown in a mixed solution, containing 0.4 g potassium titanium oxide oxalate dehydrate (PTO), 15 mL diethylene glycol (DEG) and 5 mL water at 180 °C for 3 h. Then, the nanowires were annealed at 500 °C in air to crystallize TiO_2 and remove the residual DEG.

Synthesis of Core−Shell Nanoarrays via the Solvothermal Reaction. After 0.0075 mL diethylenetramine (DETA) and 0.9 mL titanium isopropoxide (TTIP) had been successively added to 21 mL isopropyl alcohol (IPA) drop by drop with gentle stirring for 30 min, this mixture was transferred to a 50 mL Teflon-lined stainless steel autoclave. Then, the annealed TNW/FTO samples were immersed in the aforementioned mixture and leaned on the wall of autoclave chamber with the **samples side facing down** and heated to 200 °C and kept for 6−24 h. Specifically, when the reaction was kept for 24 h, honeycomb-like encircled TiO_2 nanaosheets were coated on the surface of TNW backbones to form TNW@NS core−shell hybrid nanoarrays. Moreover, when the TNW/FTO samples were placed against the wall of autoclave chamber with the **samples side facing up**, a double-layered photoanode consisting of TNW@NS underlayer and yolk−shell hierarchical TiO_2 spheres (YSHTSs) top layer can be obtained. In particular, when in the absence of DETA, TiO_2 nanoparticles were uniformly covered on TNW samples to form TNW@NP core−shell hybrid nanoarrays. All the obtained samples were washed thoroughly with ethanol and water and then annealed in air at 500 °C for 2 h to improve the crystallization of TiO_2 and remove the possible organic residue. For comparison, the P25 TiO_2 nanoparticle-based photoanode with film thickness of 22 μm was prepared on FTO using the screen-printing technique.

DSSCs Fabrication. All of the TiO_2 films described above were used as photoelectrodes to fabricate DSSCs according to a previously reported procedure.[33] In detail, the TiO_2 films were immersed into a 40 mM $TiCl_4$ aqueous solution at 70 °C for 30 min. After rinsing with water and ethanol, $TiCl_4$ treated TiO_2 samples were heated in air at 500 °C for 30 min. Then, the TiO_2 films were sensitized overnight in a 0.5 mM N719 dye in acetonitrile/tert-butanol (1:1 v/v). N719-sensitized TiO_2 electrode with an active area of approximately 0.16 cm^2 was assembled together with Pt sheet counter electrode in a sandwich type. The cell internal space was filled with liquid I^-/I_3^- redox electrolyte (0.03 M I_2, 0.6 M 1-methyl-3-propylimidazolium iodide (PMII), 0.10 M guanidinium thiocyanate, and 0.5 M tertbutylpyridine in acetonitrile and valeronitrile (85:15)).

Characterization. The morphology and microstructure of nanoarrays were examnined by field emission scanning electron microscopy (FE-SEM, JSM-6330F) and transmission electron microscopy (TEM, JEOL-2010 HR). The cystallinity and phase identification of the samples was conducted by X-ray diffraction (XRD) (Bruker D8 Advance) using Cu Kα radiation (λ = 1.5418 Å). The diffused reflectance spectra of TiO_2 nanoarrays were measured on a UV/vis-NIR spectrophotometer (UV-3150). The amount of adsorbed dye was determined by immersing the films in 0.1 M NaOH aqueous solution, and monitored the concentration of desorbed dye by a UV/vis-NIR spectrophotometer (UV-3150). The photovoltaic performance of DSSCs were obtained by mesuring photocurrent density-photovoltage ($J-V$) curves using a Keithley 2400 source meter under AM 1.5 G illumination (100 mW cm^{-2}) provided by a solar light simulator (Oriel, Model: 91192). The incident light intensity was calibrated with a NREL-calibrated Si solar cell. The IPCE spectra were measured as a function of wavelength from 380 to 800 nm on the basis of a Spectral Products DK240 monochromator. The impedance tests were performed on an electrochemical workstation (Zahner, Zennium) in the dark under open circuit voltage with the frequency range from 10 mHz to 1 MHz. The magnitude of the alternative signal was 10 mV. The impedance data were analyzed by fitting an equivalent circuit on Z-view software. Intensity-modulated photocurrent/photovoltage spectroscopy (IMPS/IMVS) measurements were also carried out on an electrochemical workstation (Zahner, Zennium).

RESULTS AND DISCUSSION

The 1D TNW nanoarrays on FTO glass were prepared by hydrothermal process in PTO/DEG/water system at 180 °C for 3 h. The amount (concentration) of PTO precursor and reaction time are carefully optimized in order to obtain the loose arrangement and smooth morphology of the 1D TNW nanoarrays, which provides plenty of scope for subsequent

surface modification. As shown in Figure 1a and b, the 1D smooth TNW nanoarrays, showing a bundle-like morphology

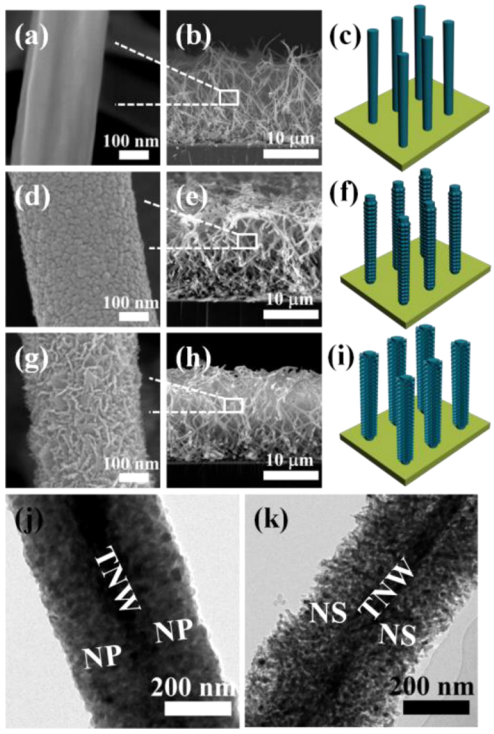

Figure 1. FE-SEM images and schematic sketches of (a, b, c) STNW; (d, e, f) TNW@NP; (g, h, i) TNW@NS. (j, k) TEM images of TNW@NP and TNW@NS.

consisting of several slim wires (70−80 nm in diameter), were vertically grown on FTO, which could be more effective in electron transport from the active layer to the FTO electrode.[33] The as-prepared TNW arrays had an average length of 16 μm (Figure 1b) and the entire diameter of 200−300 nm (Figure 1a). The preparation of TNW@NP in the absence of DETA or TNW@NS in the presence of DETA is illustrated in Figure S2 (Supporting Information). It is worth pointing out the DETA, used as a structure-directing agent, plays a pivotal role in the control of surface modification of 1D TNW scaffold, and close examination revealed that the surface of NWs experienced a smooth (Figure 1a) to rough change (Figure 1d and g) upon the subsequent modification, which in turn greatly increased the surface area of NW arrays. In the absence of DETA, the uniform coating of TiO_2 NPs on the TNW can be observed in Figure 1d. While in the presence of DETA, a large number of thin TiO_2 NSs was able to attach onto the TNW surfaces (Figure 1g). Interestingly, the cruciform NSs exhibited a good interconnectivity with each other to form a honeycomb-like network with high porosity. The outer diameter of TNW@NP and TNW@NS was increased approximately 200−300 nm (the overall diameter was ranged from 400 to 600 nm) as compared to pristine TNW backbones (Figure S1b and c, Supporting Information). Apparently, the successive solution processing does not lead to a change of total film thickness (Figure 1e and h), instead, the NPs or NSs grew on the wire surface can fill the voids between adjacent NWs. Figure 1c, f, and i give visual illustrations for three kinds of TiO_2 nanoarrays.

Moreover, the sufficient coverage of the TNW surfaces with a host of NPs or NSs to form a core−shell structure was further confirmed by TEM images in Figure 1j and k. The robust connection between core and shell layer indicates good interfacial properties between them due to homogenized TiO_2 structure. The magnified TEM images and HRTEM images of TNW@NP and TNW@NS can be shown in Figure S3 (Supporting Information). It is worth noting that each NS was composed of many small nanoparticles (6−8 nm in size, indicated by white circles, Figure S3c, Supporting Information) with oriented attachment along the epitaxial growth axis of sheets, which is smaller than that of NPs with random attachment in the case of TNW@NP (8−12 nm in size, indicated by white circles, Figure S3a, Supporting Information), indicating the important role of nanoembossed NS outer layer in enlarging the surface area for dye adsorption. In addition, the well-interconnected and interweaved NSs can form larger pores for easy electrolytes penetration. Figure S3b and d (Supporting Information) confirmed the crystal phase of NPs and NSs outer layer as pure anatase TiO_2 with a lattice spacing of 0.352 nm corresponded to the (101) crystalline plane of anatase phase. In addition, the corresponding XRD patterns (Figure S4, Supporting Information) again confirmed the anatase TiO_2 phase (JCPDS No. 21-1272) of TNW, TNW@NP, and TNW@NS, where the characteristic peaks of (101), (004), (200), (105), and (211) plane can be clearly observed. And the reinforced intensity of (101) characteristic peak for TNW@NP and TNW@NS indicates the enhanced crystallinity upon subsequent solvothermal reaction and calcination procedure.

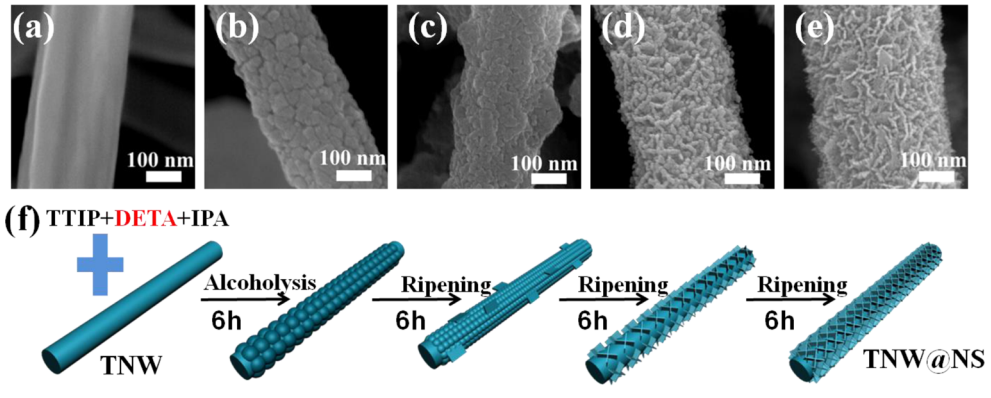

Figure 2. FESEM images of hierarchically structured TiO_2 nanoarrays prepared via TTIP/DETA/IPA solvothermal process at different reaction times: (a) 0h; (b) 6h; (c) 12h; (d) 18h; (e) 24h. (f) The schematic illustrations of the growth process of core−shell TNW@NS nanostructures.

To scrutinize the growth process of homogeneous TNW@NS yet hierarchical structure in more details, time-dependent experiments were performed. The morphologies of resulting samples were examined by SEM analysis, and the corresponding schematic illustrations of growth mechanism were also displayed in Figure 2f. After 6 h of solvothermal treatment, the originally smooth nanowires (Figure 2a) were distinctly converted into the hierarchical feature with the rough surface (Figure 2b). In this stage, large nanocrystals on the wire surface emerged from alcoholysis of TTIP in the presence of IPA and DETA which may control the alcoholysis and polycondensation process[38] and lead to an even distribution of nanocrystals around the TNW. However, the initial nanocrystals were thought to be having a poor crystalline quality and more easily redissolved. Hence, as the solvothermal treatment was proceeded to 12 h, the nanocrystals shrank over time and newly alcoholysed thorn-like nanocrystals appeared around the TNW due to the Ostwald Ripening process (Figure 2c).[39] The shell nanocrystals are not stable and will transfer from thorn shape to 2D sheet-like structure with a prolonged reaction time (>18 h), in which stage the hydrogen bonds through the unreacted amino-groups on tridentate DETA that interconnect with alcoholysis products plays an important role.[40,41] Consequently, low coverage of NSs occurs when the reaction time was progressed to 18 h (Figure 2d). Strikingly, as the growth time was further increased to 24 h, a well-developed core−shell TNW@NS nanostructure can be obtained (Figure 2e), for which the NW surfaces were entirely wrapped by a large number of interconnected NSs, leading to an interesting assembly of porous honeycomb-like shell layer on the TNW scaffolds.

The diffused reflectance ability of TNW@NP and TNW@NS was much greater than that of the pristine TNW over the whole wavelength range from 400 to 800 nm (Figure 3),

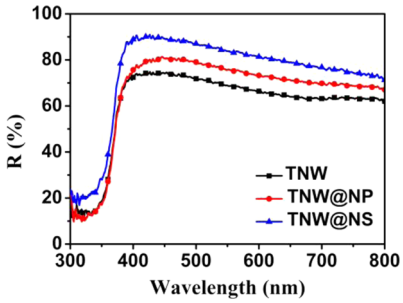

Figure 3. Diffused reflectance spectra of TNW, TNW@NP, and TNW@NS nanoarrays.

pointing out the key role of the hierarchical core−shell nanoarrays structures in dominating the light scattering behavior. The enhancement was due primarily to the increase of outer diameter of shell layer, which makes the entire size of optimized core−shell nanoarrays (400−600 nm) comparable to the wavelength of incident light in the visible range. For TNW@NP one, although good reflectance and scattering properties can be observed, it is expected that the transparency of NPs outer shell would cause the unabsorbed light to penetrate through the films without being back scattered to further enhance the light absorption. In contrast, the interconnected network of NSs on the TNW@NS nanoarrays, with a honeycomb shape and thus numerous voids, plays a role as efficient scattering elements with a high effective refractive index, which not only multireflects but also scatters the incident light of different wavelengths in the whole range of visible light.[42,43] This high scattering efficiency, would effectively multiply the optical path within the photoanode and extend the photoresponse of the photoanode to a broadband spectrum range in the visible and near-infrared regions, resulting in a significant improvement of light utilization efficiency.[7,12]

The capacity of dye loading is another key factor in determining the photovoltaic performance of DSSCs, which exerts a profound influence on the photocurrent density. In this regard, the amount of adsorbed N719 dyes was determined by adsorption−desorption measurements of sensitized TiO_2 films and the results are summarized in Table 1. The dye loading

Table 1. Detailed Photovoltaic Parameters (J_{sc}, V_{oc}, FF, and η) of DSSCs Based on Different TiO_2 Films Photoanodes under One Sun Illumination (AM 1.5G, 100 mW cm^{-2})

DSSC$_s$	J_{sc} (mA cm^{-2})	V_{oc} (mV)	η (%)	FF	adsorbed dye (nmol cm^{-2})
TNW	8.65	866	5.09	0.68	53.60
TNW@NP	13.17	815	7.38	0.69	187.5
TNW@NS	14.46	845	8.67	0.71	194.2
DL-TNW@NS-YSHTSs	17.38	825	10.01	0.70	278.6
P25	14.33	740	7.08	0.67	178.6

amount of photoanodes derived from TNW, TNW@NP, and TNW@NS were 53.6, 187.5, 194.2 nmol cm^{-2}, respectively. Clearly, all core−shell nanoarrays films (TNW@NP and TNW@NS) adsorbed more dye molecules than TNW sample, indicating the important role of NP or NS shell layer coverage in improving the surface area for greater dye loading, which would increase the probability of photon−dye interaction and thus generate higher photocurrent. In particular, TNW@NS sample showed 2.62 times higher dye loading than pristine TNW scaffold and a little higher than that of TNW@NP film due probably to smaller size of nanoparticles building units in NSs, as confirmed by the TEM analyses.

To exploit the photovoltaic applications, three different TiO_2 nanoarrays on FTO glass with similar thickness of 16 μm were used as photoanodes to assemble N719-sensitized solar cells. The photocurrent density (J_{sc})−photovoltage (V_{oc}) (J−V) characteristics of the devices were measured (Figure 4a), and the photovoltaic performance were summarized in Table 1. The markedly enhanced device performance of DSSCs prepared by utilizing core−shell hybrid arrays was clearly evidenced which mainly result from higher J_{sc} and FF. Concretely, an improved PCE of 7.38% (J_{sc} = 13.17 mA cm^{-2}, V_{oc}= 815 mV, and FF = 0.69) was achieved using TNW@NP or a more impressive PCE of 8.67% (J_{sc} = 14.46 mA cm^{-2}, V_{oc}= 845 mV, and FF = 0.71) was obtained using TNW@NS, representing a 45% or 70% increase in PCE as compared to the device based on pure TNW with PCE of 5.09% (J_{sc} = 8.65 mA cm^{-2}, V_{oc}= 866 mV, and FF = 0.68), indicating the importance of surface modification and the pivotal role of the core−shell structure. Specifically, the key to highest J_{sc} of TNW@NS based cells lies in largest amount of dye adsorption and optically optimized light scattering for the most prominent light harvesting efficiency, which is consistent with the above dye loading and reflectance analyses. Figure 4b shows the incident photon-to-current conversion efficiency (IPCE) spectra of the DSSCs with different TiO_2 nanoarrays, which reveals the IPCE values of the cells based on TNW@NP and TNW@NS photoanodes were higher than those of TNW

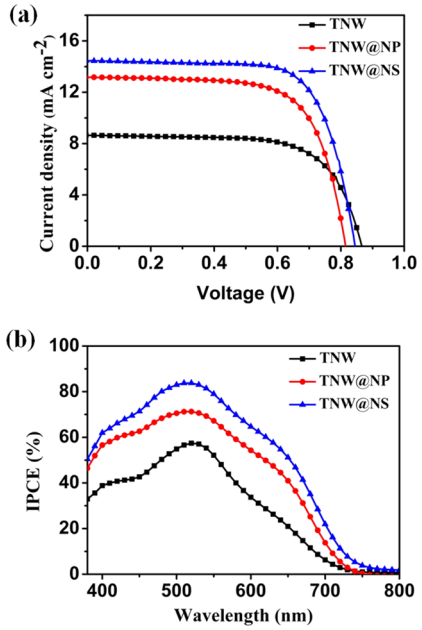

Figure 4. (a) J–V characteristics and (b) IPCE spectra of DSSCs based on TNW, TNW@NP, and TNW@NS nanoarrays photoanodes with similar film thickness of 16 μm.

cells over the whole spectra range from 400 to 800 nm, mainly due to the better dye uptakes capability and more efficient light utilization and harvesting efficiency for the core–shell arrays, resulting in enhanced J_{sc}, which is in concurrence with above J–V results.

In addition, the electrochemical impedance spectra (EIS) analysis of DSSCs fabricated with the three different TiO_2 photoanodes noted above was performed to elucidate the V_{oc} variation tendency occurred in preliminary cells tests. As shown in Figure 5, the sheet resistance (R_s) of substrate, charge

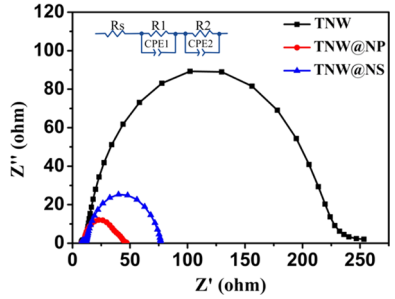

Figure 5. Nyquist plots from EIS measurement of DSSCs based on TNW, TNW@NP and TNW@NS nanoarrays photoanodes with similar film thickness of 16 μm. Inset is the simulated equivalent circuit.

transfer resistance (R_1) in the counter electrode/electrolyte interface and recombination resistance (R_2) in the TiO_2/dye/electrolyte interface can be evaluated by using an equivalent circuit containing a constant phase element (CPE) and resistances (R). In particular, the characteristics of internal charge transfer process in TiO_2/dye/electrolyte interface of the DSSCs merit attentions,[44] and the fitted resistance value (R_2) and electron lifetime (τ_r) data were accordingly showcased in Supporting Information Table S1. As shown in Figure 5 and Supporting Information Table S1, both recombination resistance value (R_2) and electron lifetime (τ_r) decreased for TNW@NP or TNW@NS based cells with respect to TNW devices, indicating much more serious charge recombination process within such cells due partially to subsequent surface modification, and this would result in the emergence of numerous grain boundaries in TiO_2 photoanodes. Especially for the TNW@NP devices, the τ_r was the smallest among all cells, which declined drastically to 52 ms as compared to 83 ms of TNW cells, mainly because the fastest recombination kinetics within the cells occurred on the random network of TiO_2 NPs outer shell, in which a host of trapping/detrapping events were present.[23,45] However, being similar as core–shell arrays structure, for the TNW@NS counterparts, an increase of τ_r to 70 ms has been witnessed (relative to TNW@NP), indicating more effectiveness of 2D NSs assembled on the TNW surface in collecting electrons from active layer to support electrode surface. Generally, the V_{oc} value of DSSCs was correlated with the charge recombination in the conduction band of TiO_2.[46,47] Accordingly, based on above analysis, a V_{oc} reduction in the order of TNW (866 mV) > TNW@NS (845 mV) > TNW@NP (815 mV) can be reasonably explicated by the different morphological structures of photoeletrodes.

Measurements of the intensity-modulated photocurrent/photovoltage spectroscopy (IMPS/IMVS) were performed to probe the intrinsic electron transport dynamics and charge recombination characteristics of the DSSCs derived from different TiO_2 nanoarrays. Typically, the electron transport time (τ_d)/lifetime (τ_r) can be derived from the IMPS/IMVS measurements according to the following equations: $\tau_d = {}^1/_{2\pi f_d}$ ($\tau_r = {}^1/_{2\pi f_r}$), where $f_d(f_r)$ is the characteristic minimum frequency of the IMPS and IMVS imaginary component.[48] Here, τ_d or τ_r provides information about the time required for the charges to exit the device or recombination with I_3^- in the electrolyte, respectively. As shown in Figure 6a and b, the shortest transport time and the highest diffusion coefficient (D_n, $D_n = d^2/(4\tau_d)$,[49] Supporting Information Figure S5) were obtained for the TNW based cell, indicating that the pure

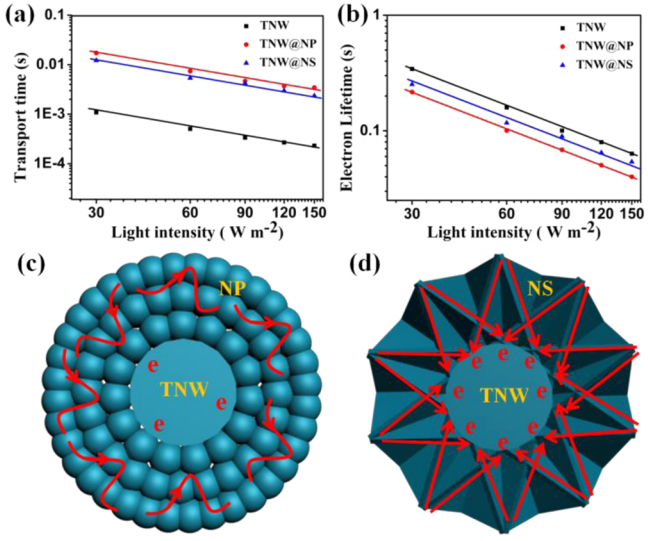

Figure 6. Time constants: (a) electron transport time and (b) electron lifetime of DSSCs based on TNW, TNW@NP, and TNW@NS photoanodes with similar film thickness of 16 μm. Schematic illustrations of electron transfer pathway and corresponding charge collection within (c) TNW@NP and (d) TNW@NS.

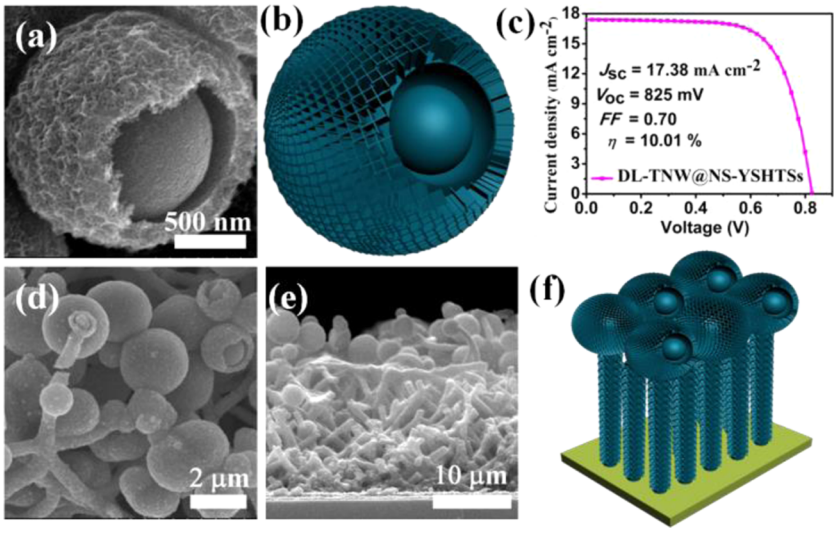

Figure 7. (a, b) SEM images and corresponding sketch of individual YSHTS. (d, e, f) Top-down, cross-sectional SEM images and according sketch of double layered TiO_2 photoanodes consisting of TNW@NS underlayer and YSHTSs top layer. (c) $J-V$ characteristics of DSSCs based on double layered TiO_2 photoanodes (16 + 6 μm).

TNW arrays are more efficient in transporting electrons due to the most direct electron transfer pathway along the y-axis, which improves the charge collection efficiency (η_{cc}, $\eta_{cc} = 1 - (\tau_d/\tau_r)$,[50] seen in Supporting Information Figure S6) and thus longest electron lifetime can be achieved.[31] While the core−shell nanoarrays (TNW@NP and TNW@NS) appear to exhibit slower electron transport and more serious charge recombination under the same illumination light intensity. This is consistent with the fact that such photoanodes yield higher surface area with a larger number of trapping sites and more complicated transfer routes. Moreover, to differentiate the photoelectric effects of NPs or NSs coverage on TNW, a schematic illustration of electron transfer pathway (ETP) viewed from the perspective of the cutting plane of TNW@NP and TNW@NS can be seen in Figure 6c and d, respectively. Specifically, for the TNW@NP, a long electron diffusion route occurred through "random walk" diffusion within the nanocrystalline outer shell layer, in which excessive trapping and detrapping events occurred within enormous defects, surface states, and grain boundaries of NPs, leading to longest electron transport time (slowest electron diffusion rate) (seen in Figure 6a and Supporting Information Figure S5) and shortest electron lifetime (fastest charge recombination rate) and thus inferior charge collection efficiency (seen in Figure 6b and Supporting Information Figure S6). While for TNW@NS, the interconnected NSs are efficient to shorten the ETP. One can see an oriented and shorted transit pathway for rapid charge transport and thus efficiently concentrate the photogenerated electrons from NS shell to TNW core. As a result, relative to TNW@NP counterpart, faster electron transport (shorter τ_d) and reduced charge recombination of electrons with oxidized species in the electrolyte (longer τ_r) and thus improved charge collection efficiency (Figure 6a, b and Supporting Information Figure S6) can be observed for TNW@NS based cells. This is likely due to the fact that the 2D well-organized NS structures on TNW should in principle navigate and quicken the transport of electron flow. Besides the inherent fast electron transfer behavior at this point it is worth noting that, as a result of higher optical density of the TNW@NS based cells due to enhanced optical properties (efficient light utilization and harvesting efficiency), the charge density at equal illumination intensity is increased for TNW@NS photoanodes, which is thought to a consequence of better saturation of trap states and thus boost electron transport to some extent.[51]

Finally, we optimized the experimental details, in which the TNW/FTO glass was placed against the wall of the autoclave chamber with the sample side facing up and then undergone the same solvothermal reaction in TTIP/DETA/IPA system (seen in Experimental Section). In this case, the TNW itself can serve as backbone for sequential surface modification, while in the mean time the facing-up placement allows the supporting of deposited resultant microspheres. Interestingly enough, the intelligent coverage of NSs on TNW surface and the deposition of microspheres on top of the nanoarrays simultaneously occurred, leading to the formation of desirable double layered TiO_2 photoanode consisting of TNW@NS under layer and yolk−shell hierarchical TiO_2 microspheres (YSHTSs) top layer. The schematic illustrations of this fabrication technique can be seen in Supporting Information Figure S7, which provides a very promising scheme and great simplicity for large-scale synthesis of double layered photoelectrode based photovoltaic devices in a cost-effective manner. It is well-known that the double-layered or multilayered assembly of the photoanode is an effective approach to significantly enhance the light trapping and scattering within the film and thus greatly improve the power conversion efficiency.[52] The SEM image (Figure 7a), sketch (Figure 7b), and the TEM images (Supporting Information Figure S8) indicates the unique yolk−shell hierarchical structures of the YSHTSs, for which the self-organized nanoembossed NSs formed the shells of the spheres in an epitaxial orientation, while the inner sphere has a much more smooth surface with closely accumulation of tiny nanocrystals. It is believed that the two kinds of hierarchical structures of the yolk and shell is beneficial to enlarge the surface area for enhanced dye-adsorption and boost the injection efficiency of the photoexcited electrons to the semiconductors.[38] In addition, the yolk−shell structure should produce a multireflection of incident light in-between the hierarchical hollow spheres, so as to improve the light harvesting efficiency.[38,53] The top-down SEM image (Figure

7d) shows a number of perfect YSHTSs with the size ranging from 1 to 2.5 μm were evenly distributed on top of the TNW@NS layer. The cross-sectional SEM image (Figure 7e) illustrates that the double layered film was composed of 16 μm thick TNW@NS under layer and 6 μm thick YSHTSs top layer (referred to here as DL-TNW@NS-YSHTSs) and the schematic sketch of such photoelectrode can be also seen in Figure 7f. For comparison, a reference P25 TiO_2 nanoparticles photoanode with similar film thickness of 22 μm was also fabricated on FTO glass via screen-printing procedure (seen in Experimental Section). These two kinds of photoanodes (DL-YSTHSs-TNW@NS and P25) were then exploited to assemble DSSC with photovoltaic parameters summarized in Table 1. After introducing of YSHTSs as an overlayer, the PCE is improved from 8.67% (TNW@NS) to 10.01% (DL-TNW@NS-YSHTSs) due to the enhanced dye adsorption and light scattering capability of the double layered TiO_2 photoelectrode.[54,55] On the other hand, one can notice that the DL-YSTHSs-TNW@NS based device shows a higher J_{sc}, V_{oc} and FF values than those of P25 cell owing to the well-organized structure composed of hierarchical core−shell arrays and yolk−shell microspheres with synergistic effects of high dye loading, superior light scattering, as well as efficient charge collection. As a result, the PCE of DSSC derived from DL-YSTHSs-TNW@NS reached 10.01% (J_{sc} = 17.38 mA cm^{-2}, V_{oc}= 825 mV, and FF = 0.70) under one sun light intensity at AM 1.5 G condition (Figure 7c) and is 41% greater than that of prototype nanoparticles counterpart (7.08%). In particular, the high V_{oc} of 825 mV for DSSCs based on 22 μm TiO_2 photoanode should be attributed to intriguing assembly of double layered TiO_2 photoanode consisting of an under layer made of well-aligned core−shell TNW@NS nanoarrays and a top layer composed of hierarchical hollow YSTHSs, where the nanoarrays on FTO substrate play pivotal roles in collecting the photogenerated electrons and the well organized hierarchical structures for both layers are beneficial to suppress the charge recombination, leading to the longer electron lifetime and thus higher V_{oc}. On balance, the complementary and synergistic properties of such intriguing assembly of double layered TiO_2 photoanode could be described as follows: an under layer made of well-aligned core−shell TNW@NS nanoarrays on FTO substrate can provide fast electron transport pathway and act as efficient charge collection medium; a top layer composed of hollow YSTHSs could offer superior light-scattering ability for enhanced light harvesting, while at the same time the hierarchical structures of both layers could guarantee better dye loading capability. Based on these preliminary results, the engineered DL-TNW@NS-YSHTSs photoanode is of practical significance in the design and fabrication of high-efficiency solar cells.

CONCLUSION

In summary, we have presented a facile solution-based method for the direct growth of well-aligned core/shell hybrid nanoarrays on TCO substrates. In this hierarchical structure, the TiO_2 nanowire core is coated with a shell of nanoparticles (TNW@NP, in the absence of DETA) or interconnected nanosheets (TNW@NS, in the presence of DETA) with a honeycomb-like porous morphology. On the basis of a time-dependent experiment, a plausible growth mechanism toward sufficient coverage of 2D nanostructures on nanowire scaffold is proposed, which involves alcoholysis and Ostwald ripening, thus leading to oriented attachment of nanosheets. The TNW@NS core−shell nanoarray has been demonstrated as an efficient light-harvesting photoanode in solar cells, yielding an excellent photovoltaic performance (8.67%) with high dye adsorption and superior light scattering ability, which could accommodate the generally incompatible factors by enhancing the surface area and efficiently collecting the electrons from shell to core simultaneously. Based on careful control of experimental condition, a novel double layered TiO_2 photoanode consisting of 16 μm thick TNW@NS under layer and 6 μm thick yolk−shell hierarchical TiO_2 microspheres (YSHTSs) top layer can be obtained, which exhibited an impressive PCE over 10% at 100 mW cm^{-2}. It is interesting to note the power conversion efficiency (10.01%) has been doubled simply through a subsequent solvothermal treatment as compared to pristine TNW scaffold (5.09%), which validates the significance and effectiveness of our proposed scheme. The markedly enhanced efficiency can be attributed to the well-organized photoanode composed of hierarchical core−shell arrays architecture and yolk−shell hollow spheres architecture with synergistic effects of high dye loading and superior light scattering for prominent light harvesting efficiency. It is envisioned that the well-aligned metal oxide based core−shell arrays architecture can be extended to other substrates or to fabricate other core−shell arrays with homogeneous or heterogeneous structures for various potential applications in electrochemical energy conversion and storage, optical devices, sensing and field emission, etc.

ASSOCIATED CONTENT

Supporting Information

FE-SEM images, schematic sketch of synthesis route, TEM and HRTEM images, XRD patterns, electron diffusion coefficient, charge collection efficiency and detailed simulative value of recombination resistance (R_2) and electron lifetime (τ_r). This material is available free of charge via the Internet at http://pubs.acs.org.

AUTHOR INFORMATION

Corresponding Author

*E-mail: kuangdb@mail.sysu.edu.cn.

Notes

The authors declare no competing financial interest.

ACKNOWLEDGMENTS

The authors acknowledge the financial supports from the NSFC (91222201, 51472274, J1103305), the Guangzhou Science and Technology Project (2014J4100016), the NSF of Guangdong Province (S2013030013474), and the Huizhou Science and Technology Project (2012C050012007).

REFERENCES

(1) Zhang, Q. F.; Cao, G. Z. Nanostructured Photoelectrodes for Dye-Sensitized Solar Cells. *Nano Today* **2011**, *6*, 91−109.

(2) Hong, Z. S.; Wei, M. D. Layered Titanate Nanostructures and Their Derivatives as Negative Electrode Materials for Lithium-Ion Batteries. *J. Mater. Chem. A* **2013**, *1*, 4403−4414.

(3) Yin, Z. Y.; Wang, Z.; Du, Y. P.; Qi, X. Y.; Huang, Y. Z.; Xue, C.; Zhang, H. Full Solution-Processed Synthesis of All Metal Oxide-Based Tree-Like Heterostructures on Fluorine-Doped Tin Oxide for Water Splitting. *Adv. Mater.* **2012**, *24*, 5374−5378.

(4) Bae, J.; Song, M. K.; Park, Y. J.; Kim, J. M.; Liu, M. L.; Wang, Z. L. Fiber Supercapacitors Made of Nanowire-Fiber Hybrid Structures

for Wearable/Flexible Energy Storage. *Angew. Chem., Int. Ed.* **2011**, *50*, 1683−1687.
(5) Lai, X. Y.; Halpert, J. E.; Wang, D. Recent Advances in Micro-/Nano-Structured Hollow Spheres for Energy Applications: From Simple to Complex Systems. *Energy Environ. Sci.* **2012**, *5*, 9944−9944.
(6) Xu, C.; Wu, J.; Desai, U. V.; Gao, D. Multilayer Assembly of Nanowire Arrays for Dye-Sensitized Solar Cells. *J. Am. Chem. Soc.* **2011**, *133*, 8122−8125.
(7) Zhang, Q. F.; Chou, T. R.; Russo, B.; Jenekhe, S. A.; Cao, G. Z. Aggregation of ZnO Nanocrystallites for High Conversion Efficiency in Dye-Sensitized Solar Cells. *Angew. Chem., Int. Ed.* **2008**, *47*, 2402−2406.
(8) Chappel, S.; Chen, S. G.; Zaban, A. A. TiO_2-coated Nanoporous SnO_2 Electrodes for Dye-Sensitized Solar Cells. *Langmuir* **2002**, *18*, 3336−3342.
(9) Tan, B.; Toman, E.; Li, Y. G.; Wu, Y. Y. Zinc Stannate (Zn_2SnO_4) Dye-Sensitized Solar Cells. *J. Am. Chem. Soc.* **2007**, *129*, 4162−4163.
(10) Chen, S. G.; Chappel, S.; Diamant, Y.; Zaban, A. Preparation of Nb_2O_5 Coated TiO_2 Nanoporous Electrodes and Their Application in Dye-Sensitized Solar Cells. *Chem. Mater.* **2001**, *13*, 4629−4634.
(11) Dong, Z. H.; Lai, X. Y.; Halpert, J. E.; Yang, N. L.; Yi, L. X.; Zhai, J.; Wang, D.; Tang, Z. Y.; Jiang, L. Accurate Control of Multishelled ZnO Hollow Microspheres for Dye-Sensitized Solar Cells with High Efficiency. *Adv. Mater.* **2012**, *24*, 1046−1049.
(12) Bai, Y.; Yu, H.; Li, Z.; Amal, R.; Lu, G. Q.; Wang, L. Z. In Situ Growth of a ZnO Nanowire Network within a TiO_2 Nanoparticle Film for Enhanced Dye-Sensitized Solar Cell Performance. *Adv. Mater.* **2012**, *24*, 5850−5856.
(13) Snaith, H. J.; Ducati, C. SnO_2-Based Dye-Sensitized Hybrid Solar Cells Exhibiting Near Unity Absorbed Photon-to-Electron Conversion Efficiency. *Nano Lett.* **2010**, *10*, 1259−1265.
(14) Ahn, S. H.; Kim, D. J.; Chi, W. S.; Kim, J. H. One-Dimensional Hierarchical Nanostructures of TiO_2 Nanosheets on SnO_2 Nanotubes for High Efficiency Solid-State Dye-Sensitized Solar Cells. *Adv. Mater.* **2013**, *25*, 4893−4897.
(15) Li, L. B.; Wang, Y. F.; Rao, H. S.; Wu, W. Q.; Li, K. N.; Su, C. Y.; Kuang, D. B. Hierarchical Macroporous Zn_2SnO_4−ZnO Nanorod Composite Photoelectrodes for Efficient CdS/CdSe Quantum Dot Co-Sensitized Solar Cells. *ACS Appl. Mater. Interfaces* **2013**, *5*, 11865−11871.
(16) Cheng, C. W.; Liu, B.; Yang, H. Y.; Zhou, W. W.; Sun, L.; Chen, R.; Yu, S. F.; Zhang, J. X.; Gong, H.; Sun, H. D.; Fan, H. J. Hierarchical Assembly of ZnO Nanostructures on SnO_2 Backbone Nanowires: Low-Temperature Hydrothermal Preparation and Optical Properties. *ACS Nano* **2009**, *3*, 3069−3076.
(17) Yang, H. G.; Sun, C. H.; Qiao, S. Z.; Zou, J.; Liu, G.; Smith, S. C.; Cheng, H. M.; Lu, G. Q. Anatase TiO_2 Single Crystals with a Large Percentage of Reactive Facets. *Nature* **2008**, *453*, 638−641.
(18) Tian, H. G.; Hu, L. H.; Zhang, C. N.; Mo, L.; Li, W. X.; Sheng, J.; Dai, S. Y. Superior Energy Band Structure and Retarded Charge Recombination for Anatase N, B Codoped Nano-Crystalline TiO_2 Anodes in Dye-Sensitized Solar Cells. *J. Mater. Chem.* **2012**, *22*, 9123−9130.
(19) Wu, W. Q.; Xu, Y. F.; Rao, H. S.; Feng, H. L.; Su, C. Y.; Kuang, D. B. Constructing 3D Branched Nanowire Coated Macroporous Metal Oxide Electrodes with Homogeneous or Heterogeneous Compositions for Efficient Solar Cells. *Angew. Chem., Int. Ed.* **2014**, *53*, 4816−4821.
(20) Lv, M.; Zheng, D.; Ye, M.; Xiao, J.; Guo, W.; Lai, Y.; Sun, L.; Lin, C.; Zuo, J. Optimized Porous Rutile TiO_2 Nanorod Arrays for Enhancing the Efficiency of Dye-Sensitized Solar Cells. *Energy Environ. Sci.* **2013**, *6*, 1615−1622.
(21) Ye, M.; Zheng, D.; Lv, M.; Chen, C.; Lin, C.; Lin, Z. Hierarchically Structured Nanotubes for Highly Efficient Dye-Sensitized Solar Cells. *Adv. Mater.* **2013**, *25*, 3039−3044.
(22) Liu, B.; Aydil, E. S. Growth of Oriented Single-Crystalline Rutile TiO_2 Nanorods on Transparent Conducting Substrates for Dye-Sensitized Solar Cells. *J. Am. Chem. Soc.* **2009**, *131*, 3985−3990.
(23) Wu, W. Q.; Rao, H. S.; Xu, Y. F.; Wang, Y. F.; Su, C. Y.; Kuang, D. B. Hierarchical Oriented Anatase TiO_2 Nanostructure Arrays on Flexible Substrate for Efficient Dye-Sensitized Solar Cells. *Sci. Rep.* **2013**, *3*, 1892.
(24) Kuang, D.; Brillet, J.; Chen, P.; Takata, M.; Uchida, S.; Miura, H.; Sumioka, K.; Zakeeruddin, S. M.; Grätzel, M. Application of Highly Ordered TiO_2 Nanotube Arrays in Flexible Dye-Sensitized Solar Cells. *ACS Nano* **2008**, *2*, 1113−1116.
(25) Varghese, O. K.; Paulose, M.; Grimes, C. A. Long Vertically Aligned Titania Nanotubes on Transparent Conducting Oxide for Highly Efficient Solar Cells. *Nat. Nanotechnol.* **2009**, *4*, 592−597.
(26) Zhuge, F. W.; Qiu, J. J.; Li, X. M.; Gao, X. D.; Gan, X. Y.; Yu, W. D. Toward Hierarchical TiO_2 Nanotube Arrays for Efficient Dye-Sensitized Solar Cells. *Adv. Mater.* **2011**, *23*, 1330−1334.
(27) Wu, W. Q.; Xu, Y. F.; Rao, H. S.; Su, C. Y.; Kuang, D. B. Multistack Integration of Three-Dimensional Hyperbranched Anatase Titania Architectures for High-Efficiency Dye-Sensitized Solar Cells. *J. Am. Chem. Soc.* **2014**, *136*, 6437−6445.
(28) Wu, W. Q.; Xu, Y. F.; Su, C. Y.; Kuang, D. B. Ultra-Long Anatase TiO_2 Nanowire Arrays with Multi-Layered Configuration on FTO Glass for High-Efficiency Dye-Sensitized Solar Cells. *Energy Environ. Sci.* **2014**, *7*, 644−649.
(29) Ye, M. D.; Xin, X. K.; Lin, C. J.; Lin, Z. Q. High Efficiency Dye-Sensitized Solar Cells Based on Hierarchically Structured Nanotubes. *Nano Lett.* **2011**, *11*, 3214−3220.
(30) Wang, J.; Lin, Z. Q. Dye-Sensitized TiO_2 Nanotube Solar Cells with Markedly Enhanced Performance via Rational Surface Engineering. *Chem. Mater.* **2010**, *22*, 579−584.
(31) Bierman, M. J.; Jin, S. Potential Applications of Hierarchical Branching Nanowires in Solar Energy Conversion. *Energy Environ. Sci.* **2009**, *2*, 1050−1059.
(32) Liao, J. Y.; Lei, B. X.; Chen, H. Y.; Kuang, D. B.; Su, C. Y. Oriented Hierarchical Single Crystalline Anatase TiO_2 Nanowire Arrays on Ti-Foil Substrate for Efficient Flexible Dye-sensitized Solar Cells. *Energy Environ. Sci.* **2012**, *5*, 5750−5757.
(33) Wu, W. Q.; Lei, B. X.; Rao, H. S.; Xu, Y. F.; Wang, Y. F.; Su, C. Y.; Kuang, D. B. Hydrothermal Fabrication of Hierarchically Anatase TiO_2 Nanowire Arrays on FTO Glass for Dye-Sensitized Solar Cells. *Sci. Rep.* **2013**, *3*, 1352.
(34) Roh, D. K.; Chi, W. S.; Jeon, H.; Kim, S. J.; Kim, J. H. High Efficiency Solid-State Dye-Sensitized Solar Cells Assembled with Hierarchical Anatase Pine Tree-Like TiO_2 Nanotubes. *Adv. Funct. Mater.* **2014**, *24*, 379−386.
(35) Sauvage, F.; Di Fonzo, F.; Bassi, A. L.; Casari, C. S.; Russo, V.; Divitini, G.; Ducati, C.; Bottani, C. E.; Comte, P.; Grätzel, M. Hierarchical TiO_2 Photoanode for Dye-Sensitized Solar Cells. *Nano Lett.* **2010**, *10*, 2562−2567.
(36) Wu, W. Q.; Feng, H. L.; Rao, H. S.; Xu, Y. F.; Kuang, D. B.; Su, C. Y. Maximizing Omnidirectional Light Harvesting in Metal Oxide Hyperbranched Array Architectures. *Nat. Commun.* **2014**, *5*, 3968.
(37) Scolan, E.; Sanchez, C. Synthesis and Characterization of Surface-Protected Nanocrystalline Titania Particles. *Chem. Mater.* **1998**, *10*, 3217−3223.
(38) Fang, W. Q.; Yang, X. H.; Zhu, H. G.; Li, Z.; Zhao, H. J.; Yao, X. D.; Yang, H. G. Yolk@shell Anatase TiO_2 Hierarchical Microspheres with Exposed {001} Facets for High-Performance Dye Sensitized Solar Cells. *J. Mater. Chem.* **2012**, *22*, 22082−22089.
(39) Wang, Y.; Yang, W.; Shi, W. Preparation and Characterization of Anatase TiO_2 Nanosheets-Based Microspheres for Dye-Sensitized Solar Cell. *Ind. Eng. Chem. Res.* **2011**, *50*, 11982−11987.
(40) Chen, J. S.; Tan, Y. L.; Li, C. M.; Cheah, Y. L.; Luan, D. Y.; Madhavi, S.; Boey, F. Y. C.; Archer, L. A.; Lou, X. W. Constructing Hierarchical Spheres from Large Ultrathin Anatase TiO_2 Nanosheets with Nearly 100% Exposed (001) Facets for Fast Reversible Lithium Storage. *J. Am. Chem. Soc.* **2010**, *132*, 6124−6130.
(41) Chen, J. S.; Luan, D. Y.; Li, C. M.; Boey, F. Y. C.; Qiao, S. Z.; Lou, X. W. TiO_2 and SnO_2@TiO_2 Hollow Spheres Assembled from Anatase TiO_2 Nanosheets with Enhanced Lithium Storage Properties. *Chem. Commun.* **2010**, *46*, 8252−8254.

(42) Qian, J. F.; Liu, P.; Xiao, Y.; Jiang, Y.; Cao, Y. L.; Ai, X. P.; Yang, H. X. TiO_2-Coated Multilayered SnO_2 Hollow Microspheres for Dye-Sensitized Solar Cells. *Adv. Mater.* **2009**, *21*, 3663−3667.
(43) Hore, S.; Nitz, P.; Vetter, C.; Prahl, C.; Niggemann, M.; Kern, R. Scattering Spherical Voids in Nanocrystalline TiO_2—Enhancement of Efficiency in Dye-Sensitized Solar Cells. *Chem. Commun.* **2005**, *41*, 2011−2013.
(44) Van de Lagemaat, J.; Park, N. G.; Frank, A. J. Influence of Electrical Potential Distribution, Charge Transport, and Recombination on the Photopotential and Photocurrent Conversion Efficiency of Dye-sensitized Nanocrystalline TiO_2 Solar Cells: A Study by Electrical Impedance and Optical Modulation Techniques. *J. Phys. Chem. B* **2000**, *104*, 2044−2052.
(45) Wu, W.-Q.; Liao, J.-Y.; Chen, H.-Y.; Yu, X.-Y.; Su, C.-Y.; Kuang, D.-B. Dye-Sensitized Solar Cells based on A Double Layered TiO_2 Photoanode Consisting of Hierarchical Nanowire Arrays and Nanoparticles with Greatly Improved Photovoltaic Performance. *J. Mater. Chem.* **2012**, *22*, 18057−18062.
(46) Montanari, I.; Nelson, J.; Durrant, J. R. Iodide Electron Transfer Kinetics in Dye-Sensitized Nanocrystalline TiO_2 Films. *J. Phys. Chem. B* **2002**, *106*, 12203−12210.
(47) Wang, M.; Chen, P.; Humphry-Baker, R.; Zakeeruddin, S. M.; Grätzel, M. The Influence of Charge Transport and Recombination on the Performance of Dye-Sensitized Solar Cells. *ChemPhysChem* **2009**, *10*, 290−299.
(48) Wang, H. X.; Nicholson, P. G.; Peter, L.; Zakeeruddin, S. M.; Grätzel, M. Transport and Interfacial Transfer of Electrons in Dye-Sensitized Solar Cells Utilizing a Co(dbbip)$_2$ Redox Shuttle. *J. Phys. Chem. C* **2010**, *114*, 14300−14306.
(49) Dloczik, L.; Ileperuma, O.; Lauermann, I.; Peter, L. M.; Ponomarev, E. A.; Redmond, G.; Shaw, N. J.; Uhlendorf, I. Dynamic Response of Dye-Sensitized Nanocrystalline Solar Cells: Characterization by Intensity-Modulated Photocurrent Spectroscopy. *J. Phys. Chem. B* **1997**, *101*, 10281−10289.
(50) Jennings, J. R.; Ghicov, A.; Peter, L. M.; Schmuki, P.; Walker, A. B. Dye-Sensitized Solar Cells Based on Oriented TiO_2 Nanotube Arrays: Transport, Trapping, and Transfer of Electrons. *J. Am. Chem. Soc.* **2008**, *130*, 13364−13372.
(51) Passoni, L.; Ghods, F.; Docampo, P.; Abrusci, A.; Martí-Rujas, J.; Ghidelli, M.; Divitini, G.; Ducati, C.; Binda, M.; Guarnera, S.; Li Bassi, A.; Casari, C. S.; Snaith, H. J.; Petrozza, A.; Di Fonzo, F. Hyperbranched Quasi-1D Nanostructures for Solid-State Dye-Sensitized Solar Cells. *ACS Nano* **2013**, *7*, 10023−10031.
(52) Wang, Z. S.; Kawauchi, H.; Kashima, T.; Arakawa, H. Significant Influence of TiO_2 Photoelectrode Morphology on the Energy Conversion Efficiency of N719 Dye-Sensitized Solar Cell. *Coord. Chem. Rev.* **2004**, *248*, 1381−1389.
(53) Liao, J. Y.; Lin, H. P.; Chen, H. Y.; Kuang, D. B.; Su, C. Y. High-Performance Dye-Sensitized Solar Cells Based on Hierarchical Yolk−Shell Anatase TiO_2 beads. *J. Mater. Chem.* **2012**, *22*, 1627−1633.
(54) Wu, W. Q.; Xu, Y. F.; Rao, H. S.; Su, C. Y.; Kuang, D. B. A Double Layered TiO_2 Photoanode Consisting of Hierarchical Flowers and Nanoparticles for High-Efficiency Dye-Sensitized Solar Cells. *Nanoscale* **2013**, *5*, 4362−4369.
(55) Qiu, Y. C.; Chen, W.; Yang, S. H. Double-Layered Photoanodes from Variable-Size Anatase TiO_2 Nanospindles: A Candidate for High-Efficiency Dye-Sensitized Solar Cells. *Angew. Chem., Int. Ed.* **2010**, *49*, 3675−3679.